Published in final edited form as:
J Am Soc Mass Spectrom. 2012 February ; 23(2): 191–200. doi:10.1007/s13361-011-0301-y.

Supercharging Protein Complexes from Aqueous Solution Disrupts their Native Conformations

Harry J. Sterling[†], **Alexander F. Kintzer**[†], **Geoffrey K. Feld**[†], **Catherine A. Cassou**[†], **Bryan A. Krantz**[†,+], and **Evan R. Williams**[†,*]

[†]Department of Chemistry, University of California, Berkeley, California 94720-1460

[+]Department of Molecular and Cell Biology, University of California, Berkeley, California 94720-1460

Abstract

The effects of aqueous solution supercharging on the solution- and gas-phase structures of two protein complexes were investigated using traveling-wave ion mobility-mass spectrometry (TWIMS-MS). Low initial concentrations of *m*-nitrobenzyl alcohol (*m*-NBA) in the electrospray ionization (ESI) solution can effectively increase the charge of concanavalin A dimers and tetramers, but at higher *m*-NBA concentrations, the increases in charge are accompanied by solution-phase dissociation of the dimers and up to a ~22% increase in the collision cross section (CCS) of the tetramers. With just 0.8% *m*-NBA added to the ESI solution of a ~630 kDa anthrax toxin octamer complex, the average charge is increased by only ~4% compared to the "native" complex, but it is sufficiently destabilized so that extensive gas-phase fragmentation occurs in the relatively high pressure regions of the TWIMS device. Anthrax toxin complexes exist in either a pre-channel or a transmembrane channel state. With *m*-NBA, the prechannel state of the complex has the same CCS/charge ratio in the gas phase as the transmembrane channel state of the same complex formed without *m*-NBA, yet undergoes extensive dissociation, indicating that destabilization from supercharging occurs in the ESI droplet prior to ion formation and is not a result of coulombic destabilization in the gas phase as a result of higher charging. These results demonstrate that the supercharging of large protein complexes is the result of conformational changes induced by the reagents in the ESI droplets where enrichment of the supercharging reagent during droplet evaporation occurs.

Introduction

Electrospray ionization (ESI) mass spectrometry (MS) of proteins or protein complexes results in a characteristic distribution of charge states from which information about the solution-phase conformations of the analytes can be inferred [1]. For aqueous or buffered aqueous solutions where the protein or complex has a "native" or "native-like" set of conformations, ESI typically results in narrow, low-charge distributions, whereas the distributions from solutions that are more denaturing are typically broad and high-charge. In addition to the solution-phase conformations of the analyte [2, 3], many factors can affect the ion charge state distribution, including analyte and solvent basicities [4-6], solvent surface tension [7-9], and various instrument parameters [10-13]. Controlling these factors to reduce or increase ion charge can be of great analytical utility. For example, a number of methods have been shown to lower ion charge states [5, 6, 14-16], facilitating identification

[*]Address reprint requests to Prof. Evan R. Williams: Department of Chemistry, University of California, Berkeley, B42 Hildebrand Hall, Berkeley, CA 94720, Phone: (510) 643-7161, FAX: (510) 642-7714, williams@cchem.berkeley.edu.

of components from heterogeneous mixtures that can have complex mass spectra because of high peak densities.

Increasing ion charge can be highly desirable because the performance of most mass analyzers, and the efficiency of most tandem-MS techniques, improves with higher analyte charge. One method for increasing the charge states of peptides, proteins and protein complexes is the addition of a small quantity of a low-volatility "supercharging" reagent to the ESI solution [7-9, 17-34]. In both "denaturing" and "native" ESI solutions, supercharging reagents, such as *m*-nitrobenzyl alcohol (*m*-NBA) [7], can cause significant charge enhancement compared to the same solutions without the reagent. During evaporation, ESI droplets become enriched with the reagent due to their very high boiling points relative to water and/or the organic solvents and acids that are typically used [35-37]. For example, the boiling point of *m*-NBA is 177 °C at 3 Torr [38], equal to ~405 °C at 760 Torr [39]. In "denaturing" solutions containing acetic acid and relatively high concentrations of organic solvents, in which most proteins are more unfolded, these reagents increase the droplet surface tension as the more volatile components preferentially evaporate [8, 9]. This enrichment results in an ESI droplet with a higher surface tension and thus a higher charge density needed to reach the Rayleigh limit [40]. More highly charged ions can be formed from droplets with a higher charge density. In contrast, the enrichment of the supercharging reagent lowers the surface tension of droplets in purely aqueous or buffered aqueous solutions (surface tension of *m*-NBA is 50 ± 5 mN/m [8] compared to 72 mN/m at 25 °C for water [38]). In the absence of other factors that affect charging, this should cause a decrease in the analyte charge, as occurs for an amine-functionalized dendrimer, poly(propyleneimine) (DAB-16) [9], which cannot undergo significant conformational changes [41]. In contrast, when this molecule was electrosprayed from a methanol solution containing *m*-NBA (methanol surface tension = 22.1 mN/m at 25 °C [38]), the charge increased compared to the same solution without the reagent [9].

We have proposed that the increase in charge observed for protein and protein complexes supercharged from purely aqueous or buffered aqueous solutions results primarily from chemical and/or thermal denaturation of the analyte that occurs *in the ESI droplet* during solvent evaporation, and that the charge enhancement from the conformational changes of the analyte can overcome the charge-reducing effects of lower droplet surface tension [19-23]. Using circular dichroism spectroscopy (CD) to monitor the transition of equine myoglobin from folded to unfolded states, the denaturing strength of sulfolane, a compound found by Loo and coworkers to be an effective supercharging reagent [24], was measured to be ~1.5 kcal/mol/M at 25 °C, which is ~30% as effective as guanidinium chloride (a common denaturant in protein folding studies) for unfolding this protein [21]. In addition, the denaturing strength of sulfolane increases at higher temperatures [21]. Reagent enrichment increases the ESI droplet lifetime [35], which should result in an increased number of collisions with neutral gas molecules in the atmosphere/vacuum interface. This should in turn reduce the rate of evaporative cooling and increase the effective temperature of the droplet [19]. In addition to CD [21, 22], results from experiments using thermal activation [19], hydrogen/deuterium exchange-MS [22, 23], traveling wave ion mobility-MS (TWIMS) [22, 23], and chemical cross-linking [20] are consistent with the hypothesis that chemical and/or thermal denaturation of the analyte in the ESI droplet is the primary origin of aqueous solution supercharging of proteins and complexes.

Here, we use TWIMS-MS to examine the effects that low initial concentrations of *m*-NBA have on the solution- and gas-phase conformations of the dimers and tetramers of the 25 kDa protein concanavalin A and an anthrax toxin octameric complex (~630 kDa). At low initial reagent concentrations, all of the complexes can be supercharged modestly, but at higher initial reagent concentrations, all of the complexes undergo disruptions of the native

conformations that manifest as either solution- or gas-phase dissociation or as an increase in their collision cross sections.

Experimental

Mass spectra and TWIMS arrival time distributions were acquired using a hybrid quadrupole/ion mobility/time-of-flight instrument (Synapt™ G2 High Definition Mass Spectrometer; Waters, Milford, MA, USA) equipped with a Z-spray ion source. Ions were formed using nanoelectrospray emitters prepared by pulling borosilicate capillaries (1.0 mm o.d./0.78 mm i.d., Sutter Instruments, Novato, CA, USA) to a tip i.d. of ~1 μm with a Flaming/Brown micropipette puller (Model P-87, Sutter Instruments, Novato, CA, USA). A platinum wire (0.127 mm diameter, Sigma, St. Louis, MO, USA) was placed in the nanoelectrospray emitter in contact with the solution, and ESI was initiated and maintained by applying ~1 kV to the wire relative to instrument ground. Solutions of concanavalin A were prepared from lyophilized protein (Sigma; used without further purification) and solutions of anthrax toxin complexes were prepared as described in detail elsewhere [42]. *m*-NBA was from Sigma and was used without further purification.

TWIMS arrival times for all ions were assigned as the center of the full-width half-maximum (FWHM) of the arrival time distribution peak. Arrival times were used to calculate the collision cross sections utilizing the calibration protocol of Bush *et al*. [43]. Homotetramers of concanavalin A and alcohol dehydrogenase and 14-mers of GroEL formed from ~10 μM solutions were used as calibrant ions. Average charge was calculated as the abundance-weighted average of each charge state in a given charge state distribution. Relative abundances of concanavalin A monomers and oligomers were calculated from the sum of the peak areas for each species, and because of differences in ionization and detection efficiencies, are only useful for comparisons of changes in their relative abundances. For concanavalin A monomer and dimer peaks that have the same *m/z*, the relative contributions of each were obtained from the normalized intensities of the TWIMS arrival time distributions.

For the concanavalin A crosslinking experiments, lyophilized protein (Sigma) was dissolved in crosslinking buffer composed of 18 mM potassium phosphate and 60 mM sodium chloride, with the pH adjusted to 6.8 with sodium hydroxide. The final protein concentration was 90 μM. An identical solution was prepared but with the addition of *m*-NBA to 1% v/v. Suberic acid bis(3-sulfohydroxysuccinimide ester) (Sigma) dissolved in extra dry DMSO (Acros Organics) was added to both solutions at a final concentration of 480 μM and allowed to react for 30 minutes at room temperature. The crosslinking reaction was quenched with the addition of ammonium acetate to a final concentration of 33 mM. The solutions were dialyzed against 20 mM ammonium acetate (pH 7.0). After dialysis, aliquots were diluted 1:10 with neat formic acid and nanoelectrosprayed directly.

Collision cross section calculations of the anthrax toxin pre-channel complexes were performed with the projection approximation algorithm in MOBCAL [44]. For the octamer pre-channel complex, $PA_8(LF_N)_4$, the crystal structure coordinates (PDB code 3KWV; [45]) were used directly in the calculation. For the heptamer pre-channel complex, $PA_7(LF_N)_3$, the calculation was performed with coordinates generated from a homology model built using COOT [46] with the crystal structure coordinates of the PA heptameric ring (PDB code 1TZO; [47]) and three LF_N molecules docked onto the ring by Least Squares Quotient alignment of PA_2LF_N ternary complexes from the $PA_8(LF_N)_4$ coordinates (PDB code 3KWV; [45]). Pre-channel and channel state models were made in CHIMERA [46] using PDB structures 3KWV and as a hybrid with 3KWV and 1V36, respectively.

Results and Discussion

Effects of Supercharging and Ionic Strength on Charge, Ion Abundance, and Collision Cross Section

Concanavalin A from *canavalia ensiformis* is a 25.6 kDa protein that reversibly self-assembles to form dimers and tetramers in relative abundances that depend on solution pH, temperature, and ionic strength [48-50]. Nanoelectrospray mass spectra of ~10 μM concanavalin A in 200 mM ammonium acetate, pH 6.8, solutions containing 0–1.5% *m*-NBA are shown in Figure 1a–d. The mass spectrum obtained from the electrospray solution without *m*-NBA (Figure 1a) is dominated by relatively narrow charge state distributions for tetramer (black triangles) and dimer (brown squares), and a low relative abundance charge state distribution for monomer (green circles). With 0.5% *m*-NBA, the average charge state for all three forms of the protein (monomer, dimer, and tetramer) increases significantly, and all three charge state distributions are broader than without *m*-NBA (Table 1; Figure 1b). Modest additional increases in average charge and range of charge states are observed for the tetramer and dimer with 1.0 and 1.5% *m*-NBA, whereas the average charge of the monomer decreases somewhat at these higher concentrations (Table 1; Figure 1c–d).

The normalized abundances of the three forms of the protein as a function of *m*-NBA concentration are shown in Figure 1e. There is a significant increase in the normalized abundance of the monomer with 1.0 and 1.5% *m*-NBA that is concomitant with a decrease in the normalized abundance of the dimer at these higher reagent concentrations. In contrast, the normalized abundance of the tetramer is essentially constant at all reagent concentrations. These results are consistent with *m*-NBA causing dissociation of the dimer into its constituent monomers. All monomer ions have the same or higher *m/z* than the dimer ions. In nozzle-skimmer dissociation experiments that cause gas-phase dissociation of native and supercharged concanavalin A dimers, the product monomer peaks are observed at higher, the same, and lower *m/z*'s than the average of the precursor dimer distribution owing to predominantly symmetric dissociation [51, 52] (Supplemental Figure 1). The higher charge state monomer ions and the absence of lower charge state monomer ions in the mass spectrum with *m*-NBA (Figure 1b-d) indicate that the dimers dissociate *in solution* and not in the gas phase where charge is conserved. It is not possible to determine from these data alone whether dissociation occurs prior to ESI or in the ESI droplets.

Previous HDX-MS and CD experiments aimed at elucidating the origin of aqueous solution supercharging show that the native structures of proteins remain intact until the concentration of the supercharging reagent is increased in the ESI droplet owing to preferential evaporation of water [21-23]. To determine if *m*-NBA affects the dimer–monomer equilibrium prior to ESI, solutions of the protein were crosslinked with suberic acid bis(3-sulfohydroxysuccinimide ester) with and without 1% *m*-NBA in the crosslinking buffer. Comparison of nanoESI mass spectra obtained for the two crosslinked protein solutions diluted to 90% formic acid to ensure complete dissociation of non-crosslinked dimers shows that the extent of crosslinking is effectively identical for the two preparations (Supplemental Figure 2). This indicates that *m*-NBA does not measurably affect the dimer–monomer equilibrium prior to ESI. Because the dimer dissociation does not occur in the gas phase, the dimer dissociation observed with *m*-NBA (Figure 1b-d) must occur in the ESI droplet.

The results of TWIMS-MS experiments in which the collision cross sections of concanavalin A tetramer ions are measured as a function of ion charge state are shown in Figure 2. For the same ion charge states formed from solutions containing different concentrations of *m*-NBA, there are only small differences in the measured collision cross sections, consistent with previous TWIMS-MS arrival time distributions of myoglobin

supercharged with *m*-NBA or sulfolane [21]. The collision cross sections of the 19+ – 25+ charge states are essentially the same, whereas for the 26+ and higher charge states, the collision cross sections increase significantly with increasing charge state. These results indicate that modest increases in charge as a result of supercharging may occur without gross conformational changes, but that beyond some threshold, which is likely protein-specific, enhanced charging may be accompanied by significant changes to the native conformations.

Less supercharging was observed for hen egg white lysozyme when this 14.3 kDa protein was electrosprayed from 200 mM ammonium acetate compared to pure water solutions using dimethyl sulfoxide as the supercharging reagent [22]. Buffers can stabilize folded forms of the protein, and may partially or fully counteract the destabilizing effects of the supercharging reagents during droplet evaporation and formation [22]. To investigate the effects of buffer concentration on the extent of supercharging of concanavalin A, nanoelectrospray mass spectra of ~10 μM concanavalin A from solutions containing 1% *m*-NBA and either 600 mM ammonium acetate, 200 mM ammonium acetate or water (all at pH 7.0) were obtained (Figure 3a-c). The average charge and width of the charge state distributions for the tetramer and dimer increase dramatically with decreasing ionic strength. The highest charge state observed for the tetramer is formed from the unbuffered solution (33+; Figure 3c) and has a collision cross section of 75.9 nm^2, which is ~22% higher than the average collision cross section of the tetramer obtained without *m*-NBA from a 200 mM ammonium acetate solution (Figure 2). The change in relative abundance of all forms of the protein as a function of *m*-NBA concentration for each of the three ionic strength solutions are shown in Figure 4. There is a significant increase in the normalized abundance of the monomer that is correlated with a decrease in ionic strength and is concomitant with a decrease in the normalized abundance of the dimer. In contrast, the normalized abundance of the tetramer does not change significantly under these solution conditions. The charge state distribution of the monomer ions relative to the charge state distribution of the dimer ions again suggests that dimer dissociation occurs *in solution* and not in the gas phase. It is not possible to determine from these experiments alone if the increases in charging with decreasing ionic strength are due to dimer and tetramer destabilization, or if other factors such as competition for charge with ammonia in the gas phase or decreased droplet charge due to charge carrier emission [53, 54], are also limiting the extent of supercharging. However, these results suggest that the buffer concentration should be minimized when maximum charging with supercharging reagents is desired.

There are a significantly higher number of intermolecular hydrogen bonds (52 vs. 14) and salt bridges (12 vs. 0) for the tetramer compared to the dimer based on the protomer binding information obtained from the crystal structure of concanavalin A [55]. This should lead to a larger activation barrier for dissociation of the tetramer compared to the dimer, consistent with the absence of tetramer dissociation and the extensive dimer dissociation observed in these experiments. Both thermodynamic [48, 49] and crystallographic [55] evidence suggest that the dimer-dimer binding interface of the tetramer is large and hydrophobic. If solvent molecules are sufficiently excluded from this binding interface before and during ESI, then the effectiveness of the supercharging reagent as a denaturant may also be reduced [20-23], consistent with the relatively modest extent of supercharging and the absence of tetramer dissociation observed in these experiments.

Complex Destabilization is Not Always Indicated by a Change in Collision Cross Section

Bacillus anthracis produces a binary toxin complex that assembles via heptameric [56] and octameric [57] ring-shaped homooligomers of the protective antigen protein (PA). These complexes can form in solution or on host cell surfaces [57]. Proteolytic activation of the ~83 kDa PA results in loss of a ~20 kDa fragment and PA oligomerizes into either a

heptameric [58] or octameric pre-channel complex [57]. Loss of the 20 kDa fragment exposes binding sites for the two other enzyme components of anthrax toxin, called lethal factor (LF) and edema factor (EF). These heptameric and octameric PA complexes can bind up to three or four copies of LF and EF, respectively [45, 57]. Following endocytosis, the PA oligomer undergoes an acidic pH induced conformational transition into its translocase channel state [59]. The enzyme factors, LF and EF, are then trafficked across the cell membrane into the cytosol where they disrupt normal cellular function [60].

Nanoelectrospray mass spectra of ~10 μM octamer-enriched PA oligomers bound to ~31 kDa PA-binding domain of LF (LF_N) [61] from 200 mM ammonium acetate, pH 7.8, solutions containing 0–0.8% *m*-NBA are shown in Figure 5. All ions of the subcomplexes and protein monomers were removed in the quadrupole by allowing only ions with $m/z >$ 8000 to travel to the IMS and TOF regions of the Synapt G2 instrument [62] used to obtain these data. Without *m*-NBA in the solution, the spectrum is dominated by a single narrow charge state distribution for the octameric complex, with a much lower relative abundance charge state distribution for the heptameric complex (Figure 5a). The abundance-weighted average collision cross sections for the octameric and heptameric complexes are 185 and 163 nm^2, respectively, both of which are 95% of their calculated collision cross section using the projection approximation algorithm in MOBCAL [44] with the crystal structure coordinates of the octameric complex [45] and a homology model of the heptameric complex. The good agreement between the measured and calculated collision cross section suggests that these complexes do not undergo gross conformational changes during ESI or in transit to the ion mobility cell [63]. With 0.4% *m*-NBA in the electrospray solution, the average charge for the octameric complex increases modestly from 49.0+ to 50.5+ and the average collision cross section also increases slightly from 185 to 187 nm^2. There is a significant decrease in ion abundance for the heptameric complex so that it is not possible to measure the average charge or collision cross section. A small population of high-charge LF_N monomers are observed in the range m/z 1200–1800. With 0.8% *m*-NBA in the electrospray solution, there is a dramatic decrease in abundance for the octameric complex and a significant increase in the abundance of the high-charge LF_N ions (Figure 5c). There is also a low relative abundance charge state distribution corresponding to a PA_2LF_N subcomplex in the range m/z 3600–4600. These lower mass LF_N monomer and subcomplex ions must be the products of gas-phase dissociation in a region of the instrument beyond the mass-filtering quadrupole ($m/z > 8000$). The average charge of the small population of octameric complexes that survives intact (Figure 5c inset) is 50.8+ and the average collision cross section is 185 nm^2.

In contrast to the solution-phase dissociation caused by *m*-NBA for supercharged concanavalin A dimers, a significant population of the supercharged octameric complex survives intact long enough to pass the mass filtering quadrupole but then dissociates in the gas phase, most likely in the relatively high-pressure regions of the ion mobility section of the instrument as a result of unintentional collisional activation. The small population of octameric complexes that survives intact has essentially the same average charge as those from the 0.4% *m*-NBA solution (50.8+ vs. 50.5+) and a slightly lower average collision cross section (185 nm^2 vs. 187 nm^2). These results indicate that only very small changes in the rotationally-averaged size of the complex ion occur as a result of the *m*-NBA enrichment, whereas the extensive gas-phase dissociation of the intact octamer indicates that the native structure and subunit interactions are significantly destabilized. This destabilization could occur first in the ESI droplet as a result of *m*-NBA-induced chemical and/or thermal denaturation [19-23], followed by either metastable or collisionally-activated dissociation (CAD) after the mass-filtering quadrupole.

To determine if destabilization occurs instead as result of increased coulombic repulsion *after* the higher charge state ions are formed, the average charge of the octamer complex was increased by inducing a specific conformational change in the complex that occurs away from the PA–ligand binding interface [42], where the vast majority of dissociation occurs for the supercharged complex. TWIMS-MS spectra of these complexes were acquired with the same instrument conditions but without *m*-NBA. The conformational transition of anthrax toxin complexes from the cell-surface pre-channel state to the transmembrane channel state was revealed in previous MS experiments by a subtle increase in the average and maximum charge in the pH range 7.2 – 7.0 that occurs without a shift in the charge states of the subcomplexes or constituent monomers, indicating a specific conformational change of the complex rather than just pH-induced unfolding [42]. The transition midpoint observed using electron microscopy (EM) and CD was also in the pH range 7.2 – 7.0 [42]. Here, the pH titration was performed with the same octamer-enriched sample of anthrax toxin and with the same instrument conditions as was used in the supercharging experiments, but without *m*-NBA. Nanoelectrospray mass spectra obtained from the pH 7.2 and 7.0 solutions (Figure 6) show a subtle increase in the average charge at the lower pH without any significant changes to the complex abundance or additional gas-phase fragmentation. Mass spectra from the pH 7.8–7.2 solutions are all essentially identical, and mass spectra from the pH 7.0–6.6 solutions are also all essentially identical (Supplemental Figure 3). The low abundance LF_N monomers are present in all spectra from pH 7.6–6.6 with approximately equal signal/noise. A plot of the average charge and average collision cross section as a function of pH is shown in Figure 6c, which demonstrates that the shift to modestly higher charge states between pH 7.2 and 7.0 is concomitant with an overall *compaction* of the complex as measured by a subtle *decrease* in the collision cross section. This is an interesting result because higher charge states for proteins are normally associated with more unfolded or elongated structures, but in this case, the rotationally-averaged size becomes more compact and results in higher charging. The oligomer in the prevailing model for the structure of the PA channel forms an approximately 100-Å long β-barrel domain [42, 64], and this extended domain appears to be able to accommodate more charges (Figure 6 inset).

The gas-phase structures of the channel state of the toxin complex are somewhat more compact than the supercharged pre-channel state complex (183 nm^2 vs. 185 nm^2, respectively), with marginally lower average charge (50.5+ vs. 50.8+, respectively). The ratio of collision cross section/charge is the same for these two forms of the complex (3.6 nm^2/z), indicating that the coulombic repulsion should be essentially the same for the channel state complex and the supercharged pre-channel complex. However, the *extensive* dissociation observed with supercharging of the pre-channel complex is not observed in any of the channel complex spectra (Supplemental Figure 3). This demonstrates that dissociation of LF_N from the supercharged pre-channel toxin complex does not occur as a result of increased coulombic repulsion, but rather as a result of destabilization that occurs prior to ion formation, similar to the destabilization that occurs for concanavalin A dimers.

Chemical and/or Thermal Destabilization in the ESI Droplet

All of the results of our studies aimed at elucidating the origin of aqueous solution supercharging have supported the hypothesis that the broad distribution of high charge ions observed with “native” protein and complex supercharging are caused by chemical and/or thermal denaturation of the analyte in the ESI droplet as the reagent concentration increases due to preferential evaporation of the solvent [19-23]. The TWIMS-MS results presented here indicate that chemical and/or thermal “destabilization” can occur without an extensive unfolding process. This destabilization must be sufficient for accommodation of additional

charges, but may not necessarily result in significant changes to the rotationally averaged size of the ion after its formation.

The pre-channel to channel transition for anthrax toxin complexes occurs with a significant change in their solution-phase structures [42, 64-66]. Nonetheless, only a modest ~1% decrease in the collision cross section (Figure 6c) was measured for the octamer channel compared to the octamer pre-channel. This illustrates that significant changes in solution-phase structures do not always result in significant changes in the collision cross section. Similarly, supercharged pre-channel complexes have essentially unchanged collision cross sections compared to native pre-channel complexes, but the extensive gas-phase dissociation of the former clearly indicates that *m*-NBA causes destabilization of its native structure that is not related to an increase in columbic repulsion after ion formation. Only the highest charge concanavalin A tetramers had measurably different collision cross sections (Figure 2), yet the dramatic dissociation of the dimers *in the ESI droplet* (Figure 3) clearly indicates that *m*-NBA is affecting the native dimer–monomer equilibrium.

Native solution supercharging of proteins and protein complexes has been used in a variety of studies, including comparisons of collision cross sections, CAD fragmentation pathways, and dissociation energies as a function of charge state [30]; attempts to map the binding sites of a cofactor [31] or ligands [32] utilizing top-down dissociation techniques; and for small molecule screening [33]. In each of these studies, the structures of the analytes formed by supercharging were assumed to be the same as those originating from buffered solutions without the supercharging reagent. The results described here show that this may not always be the case, and that the potential for destabilization or more significant denaturation and unfolding of the analyte [19-23] should be considered when supercharging reagents are used.

Conclusions

The results of these TWIMS-MS studies of supercharged concanavalin A oligomers and anthrax toxin octamer indicate that charge enhancement is the result of destabilization of the native solution-phase structures that may or may not be reflected as changes in the collision cross sections of the gas-phase ions. Similar to what occurs with monomeric proteins, this destabilization appears to happen in the ESI droplet as water preferentially evaporates and the droplet becomes enriched in the high-boiling point reagent, which then acts as a chemical denaturant [19-23]. Concanavalin A oligomers are supercharged to a much greater extent in water versus 200 and 600 mM ammonium acetate solutions, concomitant with much more extensive solution-phase dissociation of the dimer and denaturation of the tetramer. Further elucidation of the role of salts in charging [67] and supercharging is required, but these results indicate that buffer or other salt concentrations should be minimized where maximum charge through the use of supercharging reagents is desired.

Despite the destabilization inherent to aqueous solution supercharging, this technique has potential for the development or improvement of ESI-MS applications that provide information about the structures, structural transitions, and dynamics of biomolecules and their complexes in solution [23, 32] and in the gas phase [31]. In applications in which rapid unfolding and/or subunit dissociation is desired but supercharging reagents are not sufficiently denaturing on the timescale of ESI, it may be possible to use low concentrations of some Hoffmeister salts to partially destabilize the equilibrium conformations prior to, and during, ESI and/or to introduce acid vapors in the countercurrent drying gas to lower the droplet pH during ESI, as demonstrated by McLuckey and coworkers [68]. This latter technique also works best in unbuffered solutions [68], so it should be particularly effective when combined with native supercharging from unbuffered solution.

Supplementary Material

Refer to Web version on PubMed Central for supplementary material.

Acknowledgments

The authors thank the National Institutes of Health (training grants T32GM008295 for H.J.S. and T32GM066698 for A.F.K., and grants R01-AI077703 for B.A.K and R01GM096097 for E.R.W.) for generous financial support, and thank Prof. Ewa Witkowska and Dr. Haichuan Liu at the UCSF Sandler-Moore Mass Spectrometry Core Facility for use of the Synapt G2 instrument (N.I.H. grant 1S10RR029446-01).

References

1. Dobo A, Kaltashov IA. Detection of Multiple Protein Conformational Ensembles in Solution Via Deconvolution of Charge-State Distributions in ESI MS. Anal Chem. 2001; 73:4763–4773. [PubMed: 11681449]
2. Chowdhury SK, Katta V, Chait BT. Probing Conformational Changes in Proteins by Mass Spectrometry. J Am Chem Soc. 1990; 112:9012–9013.
3. Loo JA, Loo RRO, Udseth HR, Edmonds CG, Smith RD. Solvent-Induced Conformational Changes of Polypeptides Probed by Electrospray-Ionization Mass-Spectrometry. Rapid Commun Mass Spectrom. 1991; 5:101–105. [PubMed: 1666527]
4. Iavarone AT, Jurchen JC, Williams ER. Effects of Solvent on the Maximum Charge State and Charge State Distribution of Protein Ions Produced by Electrospray Ionization. J Am Soc Mass Spectrom. 2000; 11:976–985. [PubMed: 11073261]
5. Loo RRO, Smith RD. Proton-Transfer Reactions of Multiply-Charged Peptide and Protein Cations and Anions. J Mass Spectrom. 1995; 30:339–347.
6. Williams ER. Proton Transfer Reactivity of Large Multiply Charged Ions. J Mass Spectrom. 1996; 31:831–842. [PubMed: 8799309]
7. Iavarone AT, Jurchen JC, Williams ER. Supercharged Protein and Peptide Ions Formed by Electrospray Ionization. Anal Chem. 2001; 73:1455–1460. [PubMed: 11321294]
8. Iavarone AT, Williams ER. Supercharging in Electrospray Ionization: Effects on Signal and Charge. Int J Mass Spectrom. 2002; 219:63–72.
9. Iavarone AT, Williams ER. Mechanism of Charging and Supercharging Molecules in Electrospray Ionization. J Am Chem Soc. 2003; 125:2319–2327. [PubMed: 12590562]
10. Benkestock K, Sundqvist G, Edlund PO, Roeraade J. Influence of Droplet Size, Capillary-Cone Distance and Selected Instrumental Parameters for the Analysis of Noncovalent Protein-Ligand Complexes by Nano-Electrospray Ionization Mass Spectrometry. J Mass Spectrom. 2004; 39:1059–1067. [PubMed: 15386746]
11. Page JS, Kelly RT, Tang K, Smith RD. Ionization and Transmission Efficiency in an Electrospray Ionization-Mass Spectrometry Interface. J Am Soc Mass Spectrom. 2007; 18:1582–1590. [PubMed: 17627841]
12. Thomson BA. Declustering and Fragmentation of Protein Ions from an Electrospray Ion Source. J Am Soc Mass Spectrom. 1997; 8:1053–1058.
13. Yang PX, Cooks RG, Ouyang Z, Hawkridge AM, Muddiman DC. Gentle Protein Ionization Assisted by High-Velocity Gas Flow. Anal Chem. 2005; 77:6174–6183. [PubMed: 16194076]
14. Scalf M, Westphall MS, Smith LM. Charge Reduction Electrospray Mass Spectrometry. Anal Chem. 2000; 72:52–60. [PubMed: 10655634]
15. Stephenson JL, McLuckey SA. Charge Manipulation for Improved Mass Determination of High-Mass Species and Mixture Components by Electrospray Mass Spectrometry. J Mass Spectrom. 1998; 33:664–672. [PubMed: 9692249]
16. Catalina MI, van den Heuvel RHH, van Duijn E, Heck AJR. Decharging of Globular Proteins and Protein Complexes in Electrospray. Chem Eur J. 2005; 11:960–968. [PubMed: 15593239]
17. Iavarone AT, Williams ER. Collisionally Activated Dissociation of Supercharged Proteins Formed by Electrospray Ionization. Anal Chem. 2003; 75:4525–4533. [PubMed: 14632060]

18. Lomeli SH, Yin S, Loo RRO, Loo JA. Increasing Charge While Preserving Noncovalent Protein Complexes for ESI-MS. J Am Soc Mass Spectrom. 2009; 20:593–596. [PubMed: 19101165]
19. Sterling HJ, Williams ER. Origin of Supercharging in Electrospray Ionization of Noncovalent Complexes from Aqueous Solution. J Am Soc Mass Spectrom. 2009; 20:1933–1943. [PubMed: 19682923]
20. Sterling HJ, Cassou CA, Trnka MJ, Burlingame AL, Krantz BA, Williams ER. The Role of Conformational Flexibility on Protein Supercharging in Native Electrospray Ionization. Phys Chem Chem Phys. 2011; 13:18288–18296. [PubMed: 21399817]
21. Sterling HJ, Daly MP, Feld GK, Thoren KL, Kintzer AF, Krantz BA, Williams ER. Effects of Supercharging Reagents on Noncovalent Complex Structure in Electrospray Ionization from Aqueous Solutions. J Am Soc Mass Spectrom. 2010; 21:1762–1774. [PubMed: 20673639]
22. Sterling HJ, Prell JS, Cassou CA, Williams ER. Protein Conformation and Supercharing with DMSO from Aqueous Solution. J Am Soc Mass Spectrom. 2011; 22:1178–1186. [PubMed: 21953100]
23. Sterling HJ, Williams ER. Real-Time Hydrogen/Deuterium Exchange Kinetics Via Supercharged Electrospray Ionization Tandem Mass Spectrometry. Anal Chem. 2010; 82:9050–9057.
24. Lomeli SH, Peng IX, Yin S, Loo RRO, Loo JA. New Reagents for Increasing ESI Multiple Charging of Proteins and Protein Complexes. J Am Soc Mass Spectrom. 2010; 21:127–131. [PubMed: 19854660]
25. Davies NW, Wiese MD, Browne SGA. Characterisation of Major Peptides in 'Jack Jumper' Ant Venom by Mass Spectrometry. Toxicon. 2004; 43:173–183. [PubMed: 15019477]
26. Kjeldsen F, Giessing AMB, Ingrell CR, Jensen ON. Peptide Sequencing and Characterization of Post-Translational Modifications by Enhanced Ion-Charging and Liquid Chromatography Electron-Transfer Dissociation Tandem Mass Spectrometry. Anal Chem. 2007; 79:9243–9252. [PubMed: 18020370]
27. Madsen JA, Brodbelt JS. Comparison of Infrared Multiphoton Dissociation and Collision-Induced Dissociation of Supercharged Peptides in Ion Traps. J Am Soc Mass Spectrom. 2009; 20:349–358. [PubMed: 19036605]
28. Sze SK, Ge Y, Oh H, McLafferty FW. Top-Down Mass Spectrometry of a 29-kDa Protein for Characterization of Any Posttranslational Modification to within One Residue. Proc Natl Acad Sci U S A. 2002; 99:1774–1779. [PubMed: 11842225]
29. Valeja SG, Tipton JD, Emmett MR, Marshall AG. New Reagents for Enhanced Liquid Chromatographic Separation and Charging of Intact Protein Ions for Electrospray Ionization Mass Spectrometry. Anal Chem. 2010; 82:7515–7519. [PubMed: 20704305]
30. Erba EB, Ruotolo BT, Barsky D, Robinson CV. Ion Mobility-Mass Spectrometry Reveals the Influence of Subunit Packing and Charge on the Dissociation of Multiprotein Complexes. Anal Chem. 2010; 82:9702–9710. [PubMed: 21053918]
31. Enyenihi AA, Yang H, Ytterberg AJ, Lyutvinskiy Y, Zubarev RA. Heme Binding in Gas-Phase Holo-Myoglobin Cations: Distal Becomes Proximal? J Am Soc Mass Spectrom. 2011; 22:1763–1770. [PubMed: 21952890]
32. Yin S, Loo JA. Top-Down Mass Spectrometry of Supercharged Native Protein-Ligand Complexes. Int J Mass Spectrom. 2011; 300:118–122. [PubMed: 21499519]
33. Regazzoni L, Bertoletti L, Vistoli G, Colombo R, Aldini G, Serra M, Carini M, Caccialanza G, De Lorenzi E. A Combined High-Resolution Mass Spectrometric and in Silico Approach for the Characterisation of Small Ligands of Beta(2)-Microglobulin. ChemMedChem. 2010; 5:1015–1025. [PubMed: 20544784]
34. Hogan CJ, Loo RRO, Loo JA, de la Mora JF. Ion Mobility-Mass Spectrometry of Phosphorylase B Ions Generated with Supercharging Reagents but in Charge-Reducing Buffer. Phys Chem Chem Phys. 2010; 12:13476–13483. [PubMed: 20877871]
35. Grimm RL, Beauchamp JL. Evaporation and Discharge Dynamics of Highly Charged Multicomponent Droplets Generated by Electrospray Ionization. J Phys Chem A. 2010; 114:1411–1419. [PubMed: 19848399]

36. Ahadi E, Konermann L. Ejection of Solvated Ions from Electrosprayed Methanol/Water Nanodroplets Studied by Molecular Dynamics Simulations. J Am Chem Soc. 2011; 133:9354–9363. [PubMed: 21591733]
37. Zhou SL, Cook KD. Probing Solvent Fractionation in Electrospray Droplets with Laser-Induced Fluorescence of a Solvatochromic Dye. Anal Chem. 2000; 72:963–969. [PubMed: 10739199]
38. Lide, DR., editor. CRC Handbook of Chemistry and Physics. 89. 2008-2009. Online
39. Goodman JM, Kirby PD, Haustedt LO. Some Calculations for Organic Chemists: Boiling Point Variation, Boltzmann Factors and the Eyring Equation. Tetrahedron Lett. 2000; 41:9879–9882.
40. Lord, Rayleigh. Phils Mag. 1882; 14:184–186.
41. Scherrenberg R, Coussens B, van Vliet P, Edouard G, Brackman J, de Brabander E, Mortensen K. The Molecular Characteristics of Poly(Propyleneimine) Dendrimers as Studied with Small-Angle Neutron Scattering, Viscosimetry, and Molecular Dynamics. Macromolecules. 1998; 31:456–461.
42. Kintzer AF, Sterling HJ, Tang II, Abdul-Gader A, Miles AJ, Wallace BA, Williams ER, Krantz BA. Role of the Protective Antigen Octamer in the Molecular Mechanism of Anthrax Lethal Toxin Stabilization in Plasma. J Mol Biol. 2010; 399:741–758. [PubMed: 20433851]
43. Bush MF, Hall Z, Giles K, Hoyes J, Robinson CV, Ruotolo BT. Collision Cross Sections of Proteins and Their Complexes: A Calibration Framework and Database for Gas-Phase Structural Biology. Anal Chem. 2010; 82:9557–9565. [PubMed: 20979392]
44. Mesleh MF, Hunter JM, Shvartsburg AA, Schatz GC, Jarrold MF. Structural Information from Ion Mobility Measurements: Effects of the Long-Range Potential. J Phys Chem. 1996; 100:16082–16086.
45. Feld GK, Thoren KL, Kintzer AF, Sterling HJ, Tang II, Greenberg SG, Williams ER, Krantz BA. Structural Basis for the Unfolding of Anthrax Lethal Factor by Protective Antigen Oligomers. Nat Struct Mol Biol. 2010; 17:1383–1390. [PubMed: 21037566]
46. Emsley P, Cowtan K. Coot: Model-Building Tools for Molecular Graphics. Acta Crystallogr Sect D: Biol Crystallogr. 2004; 60:2126–2132. [PubMed: 15572765]
47. Lacy DB, Wigelsworth DJ, Melnyk RA, Harrison SC, Collier RJ. Structure of Heptameric Protective Antigen Bound to an Anthrax Toxin Receptor: A Role for Receptor in pH-Dependent Pore Formation. Proc Natl Acad Sci U S A. 2004; 101:13147–13151. [PubMed: 15326297]
48. Huet M, Claverie JM. Sedimentation Studies of Reversible Dimer-Tetramer Transition Kinetics of Concanavalin-A. Biochemistry. 1978; 17:236–241. [PubMed: 619990]
49. Senear DF, Teller DC. Thermodynamics of Concanavalin a Dimer-Tetramer Self-Association: Sedimentation Equilibrium Studies. Biochemistry. 1981; 20:3076–3083. [PubMed: 7248268]
50. Herskovits TT, Jacobs R, Nag K. The Effects of Salts and Ureas on the Subunit Dissociation of Concanavalin-A. Biochim Biophys Acta. 1983; 742:142–154. [PubMed: 6824678]
51. Jurchen JC, Garcia DE, Williams ER. Further Studies on the Origins of Asymmetric Charge Partitioning in Protein Homodimers. J Am Soc Mass Spectrom. 2004; 15:1408–1415. [PubMed: 15465353]
52. Jurchen JC, Williams ER. Origin of Asymmetric Charge Partitioning in the Dissociation of Gas-Phase Protein Homodimers. J Am Chem Soc. 2003; 125:2817–2826. [PubMed: 12603172]
53. Hogan CJ Jr, Caroll JA, Rohrs HW, Biswas P, Gross ML. Charge Carrier Field Emission Determines the Number of Charges on Native State Proteins in Electrospray Ionization. J Am Chem Soc. 2008; 130:6926–6927. [PubMed: 18461930]
54. Hogan CJ, Carroll JA, Rohrs HW, Biswas P, Gross ML. Combined Charged Residue-Field Emission Model of Macromolecular Electrospray Ionization. Anal Chem. 2009; 81:369–377. [PubMed: 19117463]
55. Reeke GN, Becker JW, Edelman GM. Covalent and Three-Dimensional Structure of Concanavalin A IV. Atomic Coordinates, Hydrogen Bonding, and Quaternary Structure. J Biol Chem. 1975; 250:1525–1547. [PubMed: 1112816]
56. Milne JC, Furlong D, Hanna PC, Wall JS, Collier RJ. Anthrax Protective Antigen Forms Oligomers During Intoxication of Mammalian Cells. J Biol Chem. 1994; 269:20607–20612. [PubMed: 8051159]

57. Kintzer AF, Thoren KL, Sterling HJ, Dong KC, Feld GK, Tang II, Zhang TT, Williams ER, Berger JM, Krantz BA. The Protective Antigen Component of Anthrax Toxin Forms Functional Octameric Complexes. J Mol Biol. 2009; 392:614–629. [PubMed: 19627991]
58. Petosa C, Collier RJ, Klimpel KR, Leppla SH, Liddington RC. Crystal Structure of the Anthrax Toxin Protective Antigen. Nature. 1997; 385:833–838. [PubMed: 9039918]
59. Blaustein RO, Koehler TM, Collier RJ, Finkelstein A. Anthrax Toxin-Channel-Forming Activity of Protective Antigen in Planar Phospholipid-Bilayers. Proc Natl Acad Sci U S A. 1989; 86:2209–2213. [PubMed: 2467303]
60. Krantz BA, Finkelstein A, Collier RJ. Protein Translocation through the Anthrax Toxin Transmembrane Pore Is Driven by a Proton Gradient. J Mol Biol. 2006; 355:968–979. [PubMed: 16343527]
61. Lacy DB, Mourez M, Fouassier A, Collier RJ. Mapping the Anthrax Protective Antigen Binding Site on the Lethal and Edema Factors. J Biol Chem. 2002; 277:3006–3010. [PubMed: 11714723]
62. Giles K, Williams JP, Campuzano I. Enhancements in Travelling Wave Ion Mobility Resolution. Rapid Commun Mass Spectrom. 2011; 25:1559–1566. [PubMed: 21594930]
63. Ruotolo BT, Giles K, Campuzano I, Sandercock AM, Bateman RH, Robinson CV. Evidence for Macromolecular Protein Rings in the Absence of Bulk Water. Science. 2005; 310:1658–1661. [PubMed: 16293722]
64. Katayama H, Wang J, Tama F, Chollet L, Gogol EP, Collier RJ, Fisher MT. Three-Dimensional Structure of the Anthrax Toxin Pore Inserted into Lipid Nanodiscs and Lipid Vesicles. Proc Natl Acad Sci U S A. 2010; 107:3453–3457. [PubMed: 20142512]
65. Vernier G, Wang J, Jennings LD, Sun J, Fischer A, Song LK, Collier RJ. Solubilization and Characterization of the Anthrax Toxin Pore in Detergent Micelles. Prot Sci. 2009; 18:1882–1895.
66. Katayama H, Janowiak BE, Brzozowski M, Juryck J, Falke S, Gogol EP, Collier RJ, Fisher MT. GroEL as a Molecular Scaffold for Structural Analysis of the Anthrax Toxin Pore. Nat Struct Mol Biol. 2008; 15:754–760. [PubMed: 18568038]
67. Wang GD, Cole RB. Effect of Solution Ionic-Strength on Analyte Charge-State Distributions in Positive and Negative-Ion Electrospray Mass-Spectrometry. Anal Chem. 1994; 66:3702–3708.
68. Kharlamova A, Prentice BM, Huang TY, McLuckey SA. Electrospray Droplet Exposure to Gaseous Acids for the Manipulation of Protein Charge State Distributions. Anal Chem. 2010; 82:7422–7429. [PubMed: 20712348]

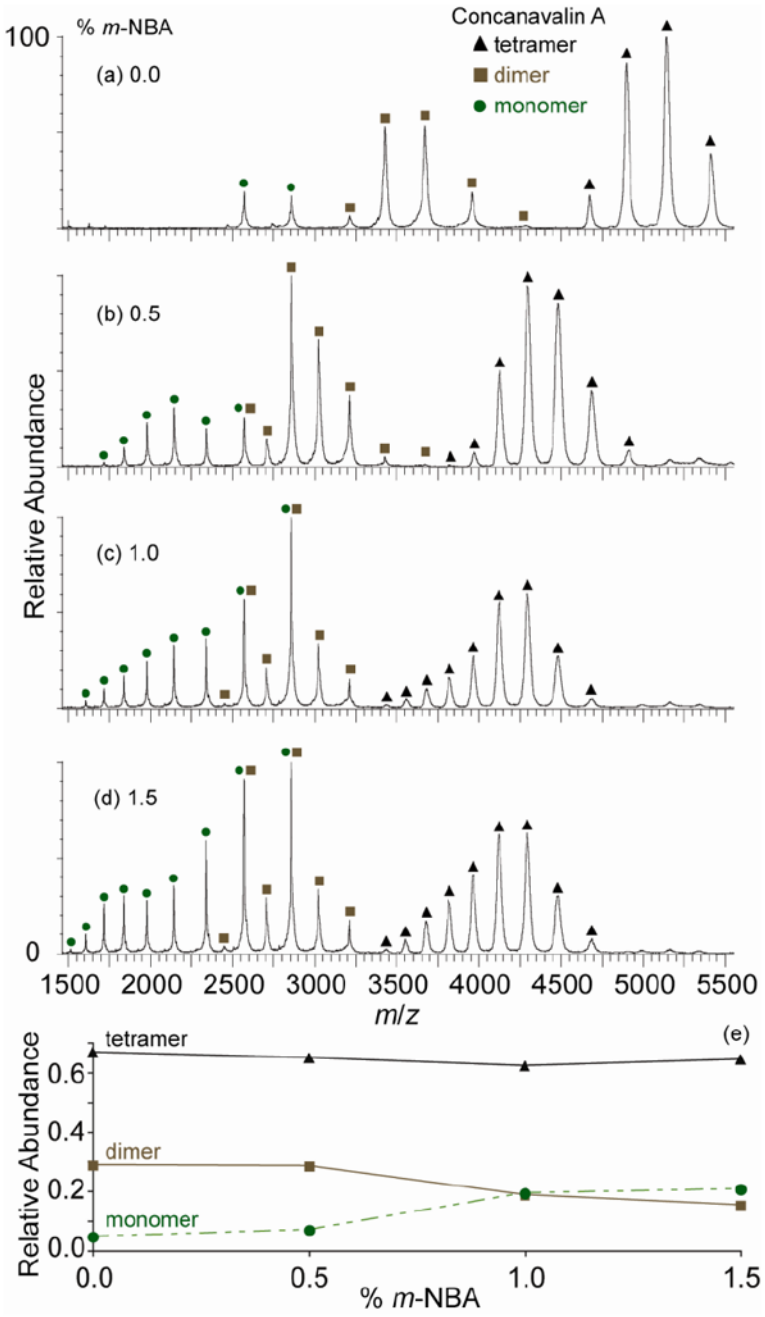

Figure 1.

Nanoelectrospray mass spectra of ~10 μM concanavalin A in 200 mM ammonium acetate, pH 6.8, aqueous solution containing (a) 0%, (b) 0.5%, (c) 1.0% and (d) 1.5% *m*-NBA. The normalized abundances of concanavalin A monomer, dimer and tetramer as a function of *m*-NBA concentration are shown in (e).

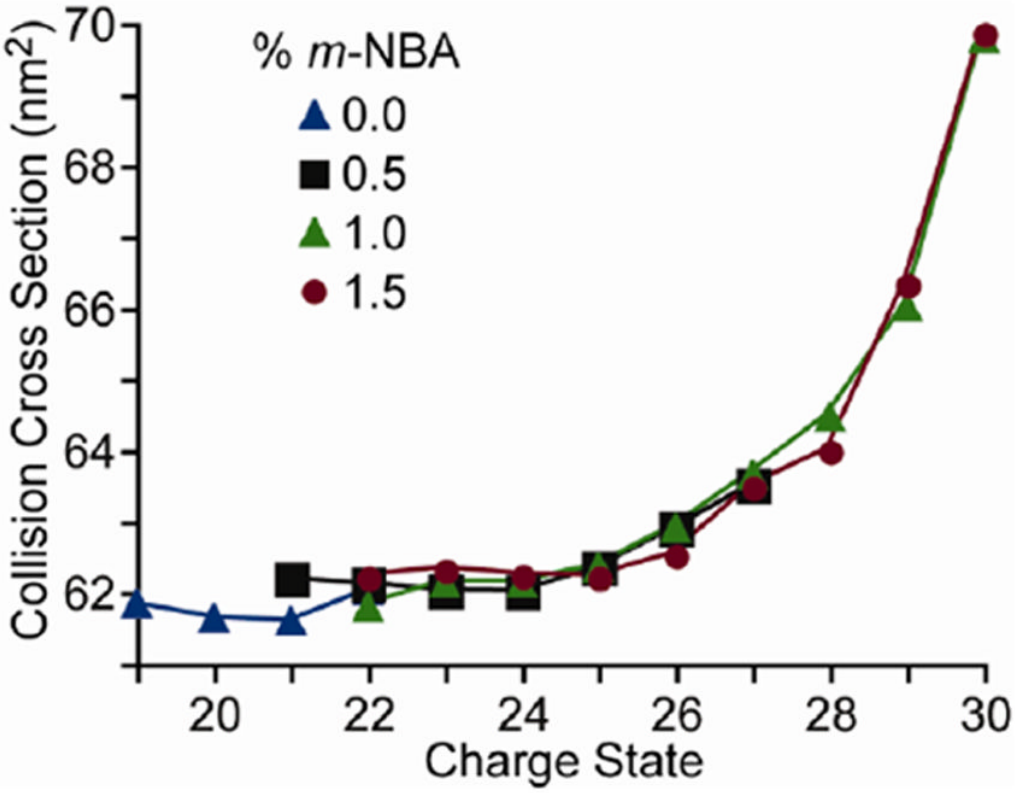

Figure 2.
Collision cross section of concanavalin A tetramers as a function of charge state for ~10 μM aqueous protein solutions containing 0–1.5% *m*-NBA.

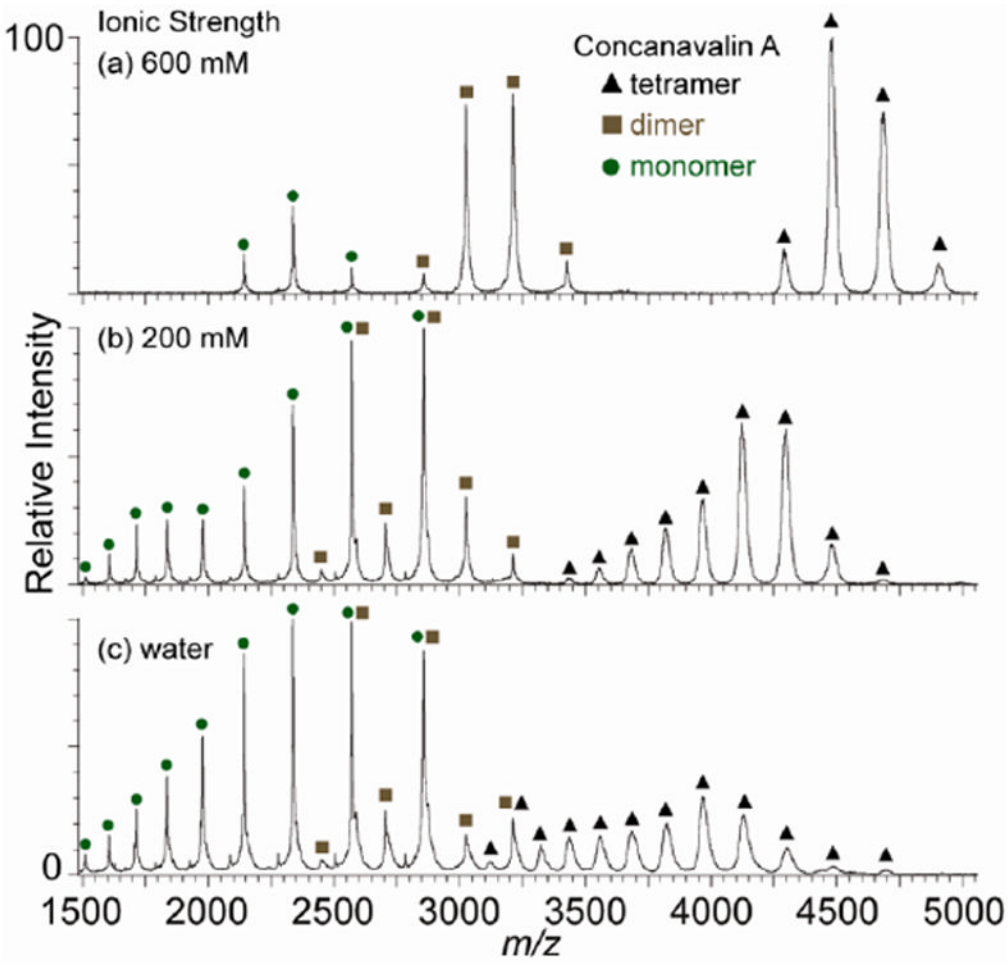

Figure 3.
Nanoelectrospray mass spectra of ~10 μM aqueous concanavalin A solutions containing 1% *m*-NBA and either (a) 600 mM ammonium acetate, (b) 200 mM ammonium acetate, or (c) water.

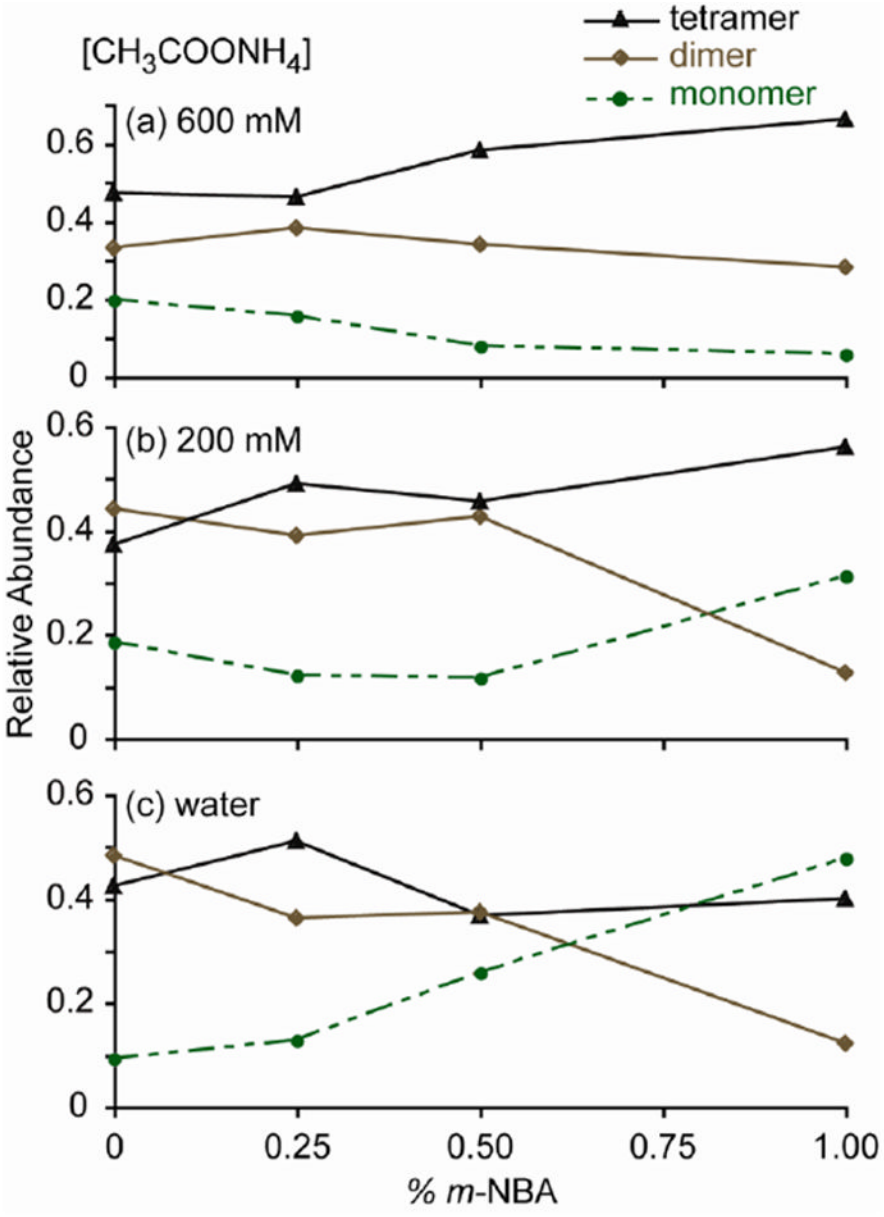

Figure 4.
Normalized abundances of concanavalin A monomer, dimer and tetramer as a function of *m*-NBA concentration for pH 7.0 aqueous solutions containing (a) 600 mM, (b) 200 mM, or (c) no ammonium acetate.

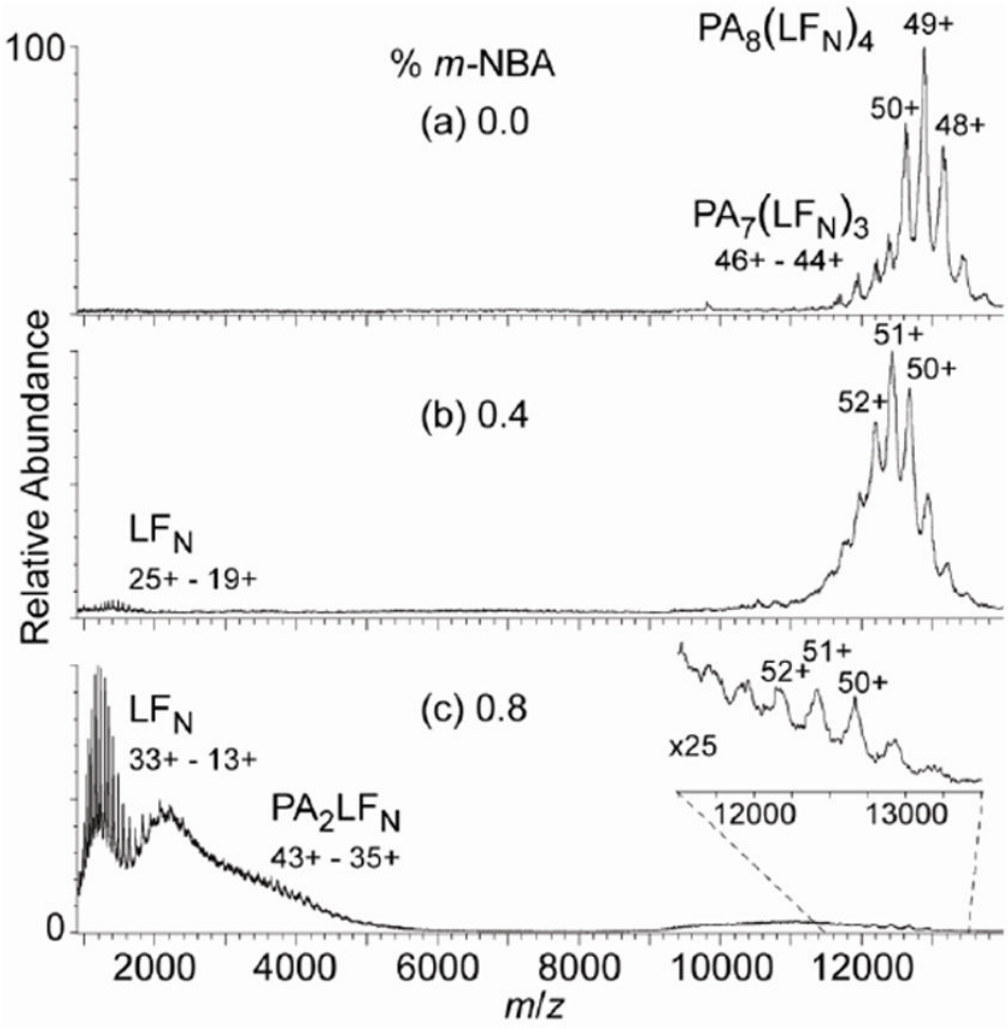

Figure 5.

Nanoelectrospray mass spectra of ~10 μM octamer-enriched PA oligomers bound to LF_N from 200 mM ammonium acetate, pH 7.8, aqueous solutions containing (a) 0%, (b) 0.4%, and (c) 0.8% *m*-NBA.

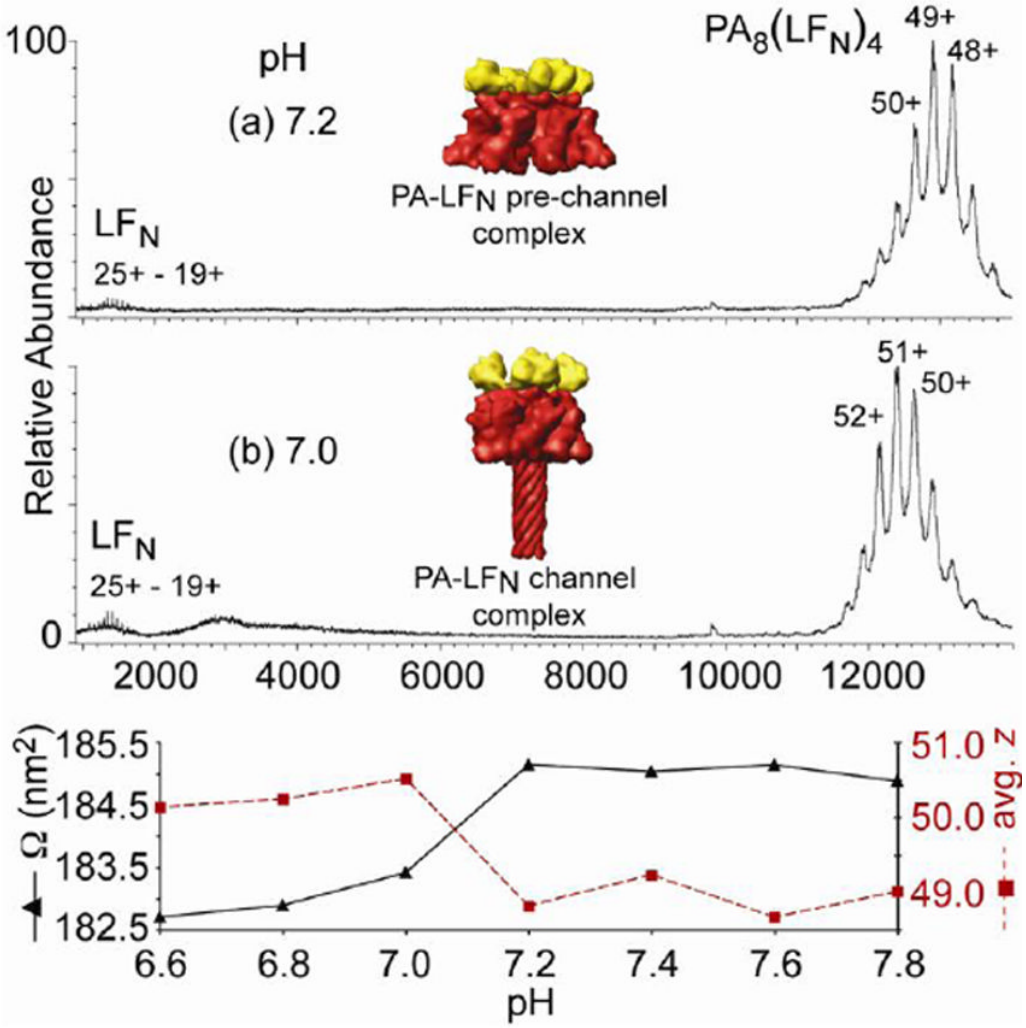

Figure 6.

Nanoelectrospray mass spectra of ~10 μM octamer-enriched PA oligomers bound to LF_N from 200 mM ammonium acetate aqeuous solutions at pH (a) 7.2 and (b) 7.0. Models of the pre-channel and channel forms of anthrax toxin complexes are inset. Plotted below the mass spectra are the average charge (red squares; right axis) and average collision cross section (black triangles; left axis) of the octamer complex as a function of solution pH.

Table 1

Average charge (and range of charge states) observed for each oligomeric state of concanavalin A nanoelectrosprayed from 200 mM ammonium acetate solutions containing 0–1.5% *m*-NBA.

	Average charge (and range of charge states) (+)			
Concanavalin A	**0%**	**0.5%**	**1.0%**	**1.5%**
tetramer	20.3 (22-9)	23.5 (27-21)	24.8 (30-22)	25.0 (30-22)
dimer	14.3 (16-3)	17.4 (20-15)	17.8 (21-16)	18.0 (21-16)
monomer	9.4 (10-8)	11.8 (15-9)	10.8 (16-9)	11.6 (17-9)